ISSN 0036-0244, Russian Journal of Physical Chemistry A, 2024, Vol. 98, No. 9, pp. 1968–1975. © Pleiades Publishing, Ltd., 2024.

TO THE CENTENARY OF THE CHEMICAL THERMODYNAMICS LABORATORY OF MOSCOW STATE UNIVERSITY

# Phase Equilibria in the $PrO_x$–$CoO_x$–NiO System, Structure, and Oxygen Content in the Formed Oxides

**E. E. Solomakhina[a,*], M. A. Shadrina[b], A. V. Bryuzgina[a,b], A. S. Urusova[a], T. V. Aksenova[a], and V. A. Cherepanov[a]**

[a] *Institute of Natural Science and Mathematics, Ural Federal University named after the first President of Russia B. N. Yeltsin, Yekaterinburg, Russia*

[b] *Institute of Solid State Chemistry Ural Branch of Russian Academy of Science, Yekaterinburg, Russia*

**e-mail: e.e.solomakhina@urfu.ru*

Received December 4, 2023; revised December 4, 2023; accepted December 20, 2023

**Abstract**—Using the homogenizing annealing method and X-ray powder diffraction, it was shown that in the quasi-ternary $PrO_x$–CoO–NiO system at 1373 K in air, two series of solid solutions are formed: $PrCo_{1-x}Ni_xO_3$ ($0.0 \le x \le 0.4$) with the orthorhombically distorted perovskite structure and $Pr_4Ni_{3-y}Co_yO_{10-\delta}$ ($0.7 \le y \le 1.5$) with the Ruddlesden–Popper type structure with $n = 3$. The oxygen content in both series of solid solutions is close to stoichiometric. It is assumed that $Ni^{2+}$ ions are predominantly located in octahedra located in the middle of the perovskite block, while $Ni^{3+}$ and $Co^{3+}$ ions are in octahedra adjacent to the rock salt layers. Phase diagrams of the $PrO_x$–$CoO_x$ and $PrO_x$–NiO systems were constructed in "*T*–composition" coordinates in air using literature data.

**Keywords:** phase equilibria, crystal structure, oxygen content

**DOI:** 10.1134/S0036024424701097

## INTRODUCTION

Rare earth nickelates with a perovskite-like structure are promising materials for use as cathodes in fuel cells [1–13]. Unlike oxide systems based on other 3*d*-transition metals (for example, Co, Fe, Mn), rare earth nickelates formed in Ni-containing systems and belonging to the Ruddlesden–Popper homologous series $Ln_{n+1}Ni_nO_{3n+1}$ can be obtained in air without introducing acceptor-type substituents into the A-sublattice (for example, alkaline earth metal cations). Among other rare earth elements, praseodymium attracts particular attention, as it exhibits high catalytic activity in redox reactions involving oxygen. Partial replacement of nickel with cobalt in the B-sublattice leads to increased stability of oxides with the $ABO_3$ perovskite structure, as well as an increase in electrical conductivity, electrochemical activity of oxides, and acceleration of oxygen exchange processes between the solid and gas phases [14–25]. However, the available information on selected compositions with the simultaneous presence of nickel and cobalt in the resulting oxides with a perovskite-like structure does not provide a complete understanding of the phase equilibria in the $PrO_x$–NiO–$CoO_x$ system. Another important parameter responsible for many functional properties is the oxygen content in the oxides. The available information concerning oxygen content in oxides in the aforementioned system is insufficient. Thus, the purpose of this work is to establish phase equilibria in the $PrO_x$–NiO–CoO system at 1373 K in air and determine the oxygen content in the resulting phases.

Phase equilibria in the constituent binary oxide systems have been studied quite well earlier.

**$PrO_x$–$CoO_x$ system.** The results of studying phase equilibria in the $PrO_x$–$CoO_x$ system [26–29] in a wide range of temperatures and oxygen pressures allow to conclude that only $PrCoO_3$ with the orthorhombically distorted perovskite structure ($a$ = 5.3390 Å, $b$ = 5.3513 Å, $c$ = 7.5762 Å, sp. gr. *Pbnm* [30]) is stable in air conditions, while other cobaltites $Pr_4Co_3O_{10}$ and $Pr_2CoO_4$, belonging to the Ruddlesden-Popper homologous series, are stable at lower oxygen pressures.

**$PrO_x$–NiO system.** The thermodynamic stability of nickelates is shifted towards higher oxygen pressures compared to cobalt-containing analogues. A single-phase oxide with a perovskite structure $PrNiO_3$, is obtained only when using oxygen pressures increased relative to air [2, 31–34], while phases with a Ruddlesden–Popper type structure, $Pr_2NiO_4$ and $Pr_4Ni_3O_{10}$, can be obtained in an air conditions [3, 5, 7, 9, 11–13, 27–29, 35]. Synthesis of $PrNiO_3$ at 973 K

in air does not allow obtaining a single-phase product; the sample contained large amounts of unreacted initial oxides $PrO_x$ and NiO [36]. The difficulty of preparing single-phase $PrNiO_3$ in air is associated with kinetic reasons, since its thermal stability at $P_{O_2}$ = 0.21 atm is limited by relatively low temperatures for solid-phase processes. The single-phase sample obtained at higher $P_{O_2}$ found to be stable in an air atmosphere up to 1223 K [2]. At approximately 873 K, $PrNiO_3$ undergoes a reversible phase transition from a high-temperature rhombohedral cell (sp. gr. *R*-3*c*) to a low-temperature orthorhombic cell (sp. gr. *Pnma*) [2]. When the temperature increased above 1223 K, at the first stage the decomposition products of $PrNiO_3$ were NiO and $Pr_4Ni_3O_{10}$, and above 1328 K, the latter, in turn, decomposed into $Pr_2NiO_4$ and NiO [2]. The stability of $Pr_2NiO_4$ at relatively low temperatures has also been the subject of researches [13, 37, 38]. The temperature of oxidative decomposition of $Pr_2NiO_4$ into $Pr_4Ni_3O_{10}$ and $PrO_x$ in air lies in the range of 1123–1173 K.

**CoO–NiO system.** A continuous series of (Co,Ni)O solid solutions is formed in the CoO–NiO system at $T > 1173$ K in air [39].

**$PrO_x$–$CoO_x$–NiO system.** Several solid solutions in which cobalt and nickel are partially substituted for each other have been previously described. There is information about oxides with the perovskite structure $PrCo_{1-x}Ni_xO_{3-\delta}$ with nickel content $x = 0.4$ [24], $x = 0.5$ [16, 20], $x = 0.6$ [18], $0 \le x \le 0.7$ [40], although not all works indicate the preparation conditions. On the side of nickelates with a Ruddlesden–Popper type structure, the oxides $Pr_4Ni_{3-y}Co_yO_{10-\delta}$ with $y = 0.3$ [25, 41] and $Pr_2Ni_{1-y}Co_yO_{4+\delta}$, with $y = 0.1$–$0.2$ [14, 15, 21, 22] have been described. The boundaries of the homogeneity ranges of existing solid solutions, which undoubtedly depend on temperature, have not been determined to date.

## EXPERIMENTAL

The samples were synthesized using the glycerol-nitrate method. Praseodymium oxide $Pr_6O_{11}$, metallic cobalt Co, and crystalline nickel acetate hydrate $Ni(CH_3COO)_2{\cdot}4H_2O$ were used as starting materials. To remove adsorbed moisture and gases, $Pr_6O_{11}$ was pre-calcined for 12 h at a temperature of 698 K; then it was removed from the heated furnace, cooled in a desiccator and weighed in closed beakers of known mass. The required masses of other components were calculated from the known mass of $Pr_6O_{11}$. Metallic cobalt was obtained by reduction of cobalt oxide $Co_3O_4$ in a hydrogen flow at 898 K. Weighed amounts of the starting components were dissolved in nitric acid when heated. An equimolar amount of glycerol was added to the resulting solution and heated until complete evaporation. The dry residue was slowly heated to 1373 K and kept at this temperature for 12 h. All subsequent anneals with intermediate grinding in ethyl alcohol after every 12 h were carried out at 1373 K. The total annealing time was 72 h. At the end of the annealing, the samples were quenched by abruptly removing them from the heated furnace onto a massive metal copper plate in air. The approximate cooling rate was 500 K/min.

The phase composition of the samples was controlled by XRD using an Inel Equinox 3000 and a Shimadzu XRD 7000 diffractometers in Cu$K_\alpha$ radiation. The structural parameters were refined using the Rietveld full-profile analysis method in the Fullprof program.

The melting points of samples in the $PrO_x$–CoO system were determined by visual polythermal analysis using a platinum/platinum-rhodium thermocouple (PP-1).

The change in oxygen content in the samples with varying temperature was determined by thermogravimetric analysis using a STA 409 PC thermal analyzer. The absolute value of oxygen content was determined by the direct reduction of samples using a mixture of gases (90% $H_2$ + 10% $N_2$) at 1373 K in a TG cell to $Pr_2O_3$ and metallic Co and Ni. The completeness of reduction at the end of the experiment was monitored by XRD.

## RESULTS AND DISCUSSION

### *Phase Diagrams of the $PrO_x$–$CoO_x$ and $PrO_x$–NiO Systems*

Although phase equilibria in the binary systems have been the subject of numerous studies, phase diagrams of these systems in air have not been presented previously. Based on our experimental data on the melting temperatures in the $PrO_x$–CoO system together with the results of homogenizing annealing at various temperatures and the available scattered literature data on the thermal stability of intermediate phases in air: $PrCoO_3$ [26–30, 40], $PrNiO_3$ [2, 10, 32, 36], $Pr_4Ni_3O_{10}$ [3, 9, 35, 41, 42], and $Pr_2NiO_4$ [5–7, 10, 13, 37, 38], we constructed phase diagrams of the $PrO_x$–$CoO_x$ and $PrO_x$–NiO systems in the "*T*–composition" coordinates in air (Figs. 1 and 2). The relative mole fraction of the metallic component is a traditional way of expressing concentration in systems where cations can reveal different oxidation states in coexisting phases at fixed *T* and/or $P_{O_2}$. The oxygen content in the condensed phases cannot be calculated from the diagram, but is assigned in accordance with its real value.

The crystal structure of $PrCoO_3$ quenched from 1373 K to room temperature was indexed in an orthorhombic cell sp. gr. *Pbnm* with unit cell parameters: $a$ = 5.3775(1) Å, $b$ = 5.3439(1) Å, $c$ = 7.5773(2) Å, which

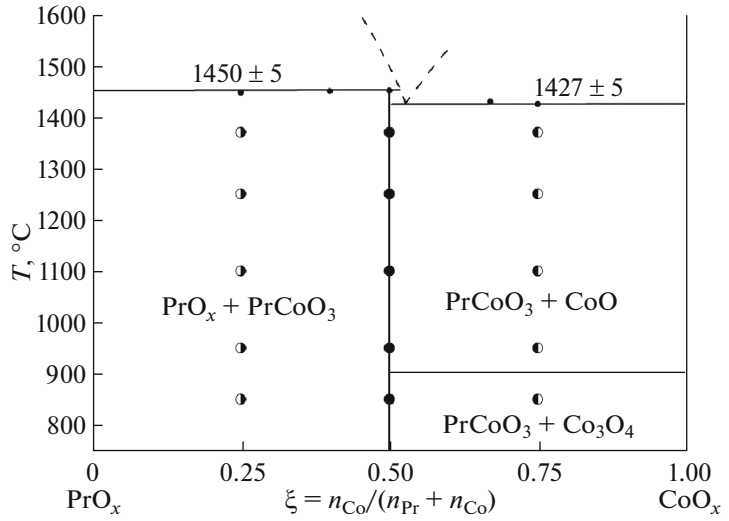


**Fig. 1.** Phase diagram of the $PrO_x$–$CoO_x$ system in air.

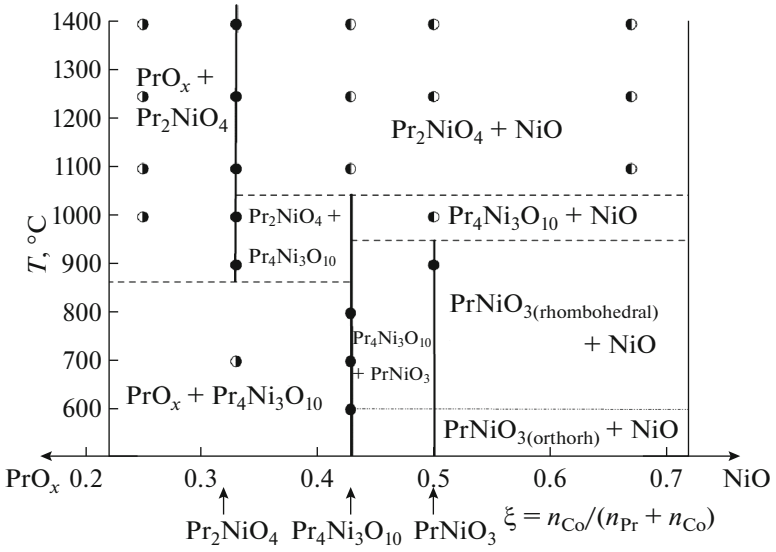


**Fig. 2.** Phase diagram of the $PrO_x$–NiO system in air.

is in good agreement with the data available in the literature [40]. The only thermodynamically stable oxide at 1373 K in the $PrO_x$–NiO system is $Pr_2NiO_4$, which crystallizes in an orthorhombic structure (sp. gr. *Fmmm*) with the unit cell parameters: $a$ = 5.3976(1) Å, $b$ = 5.4527(1) Å, $c$ = 12.4397(1) Å. After annealing at 1373 K in air the samples which overall composition corresponded to $PrNiO_3$ and $Pr_4Ni_3O_{10}$, were mixtures of two phases: $Pr_2NiO_4$ and NiO. Annealing of $Pr_2NiO_4$ in air at $T \geq 1123$ K indicates its oxidative decomposition into $Pr_4Ni_3O_{10}$ and $PrO_x$ [13, 37, 38].

### *$PrCo_{1-x}Ni_xO_3$ Solid Solutions*

XRD of samples with nominal composition $PrCo_{1-x}Ni_xO_3$ in the range $0 \leq x \leq 0.5$ ($\Delta x = 0.05$), quenched from 1373 K to room temperature, confirmed the formation of single-phase solid solutions in the composition range $0 \leq x \leq 0.4$. The structural parameters of the solid solutions are listed in Table 1. Starting from $x = 0.45$, lines of impurity phases such as Ruddlesden–Popper type with $n = 3$ and NiO were detected in the XRD patterns.

The oxygen content in all the obtained solid solutions is close to stoichiometric and practically does not

**Table 1.** Structural parameters of the $PrCo_{1-x}Ni_xO_3$ solid solution

| Sp. gr. *Pbnm:* Pr (4*c*) (*x*; *y*; 1/4), Co/Ni (4*b*) (1/2; 0; 0), O1 (4*c*) (*x*; *y*; 1/4), O2 (8*d*) (*x*; *y*; *z*) | | | | | |
|---|---|---|---|---|---|
| *x* | 0.0 | 0.1 | 0.2 | 0.3 | 0.4 |
| *a*, Å | 5.3775(1) | 5.3829(1) | 5.3875(1) | 5.3929(4) | 5.3944(2) |
| *b*, Å | 5.3439(1) | 5.3519(1) | 5.3588(1) | 5.3681(4) | 5.3669(2) |
| *c*, Å | 7.5773(2) | 7.5866(2) | 7.5942(1) | 7.6034(5) | 7.6016(3) |
| *V*, Å$^3$ | 217.75(1) | 218.56(1) | 219.25(1) | 220.11(1) | 220.08(2) |
| *x*(Pr) | –0.01123 | –0.00516 | –0.00516 | 0.00934 | 0.00293 |
| *y*(Pr) | 0.03143 | 0.03194 | 0.03194 | 0.02785 | 0.03095 |
| *x*(O1) | 0.08002 | 0.06737 | 0.07587 | 0.94724 | 0.06676 |
| *y*(O1) | 0.48768 | 0.48930 | 0.48916 | 0.48563 | 0.50289 |
| *x*(O2) | 0.70781 | 0.70649 | 0.70984 | 0.68845 | 0.72028 |
| *y*(O2) | 0.29055 | 0.28460 | 0.28575 | 0.25805 | 0.27680 |
| *z*(O2) | 0.02894 | 0.03690 | 0.03743 | 0.03815 | 0.04897 |
| $R_p$, % | 11.1 | 9.57 | 9.75 | 12.10 | 7.17 |
| $R_f$, % | 12.5 | 7.04 | 7.15 | 16.70 | 11.0 |
| $R_{Br}$, % | 12.4 | 4.97 | 4.60 | 17.30 | 10.1 |
| ρ, g/cm$^3$ | 7.560 | 7.531 | 7.507 | 7.476 | 7.494 |

change when the temperature is varied from room temperature to 1373 K, which corresponds to the oxidation state of 3+ for cobalt and nickel ions and is in good agreement with the results obtained in other works [40, 43, 44]. Practically linear increase in the unit cell parameters with increasing nickel content

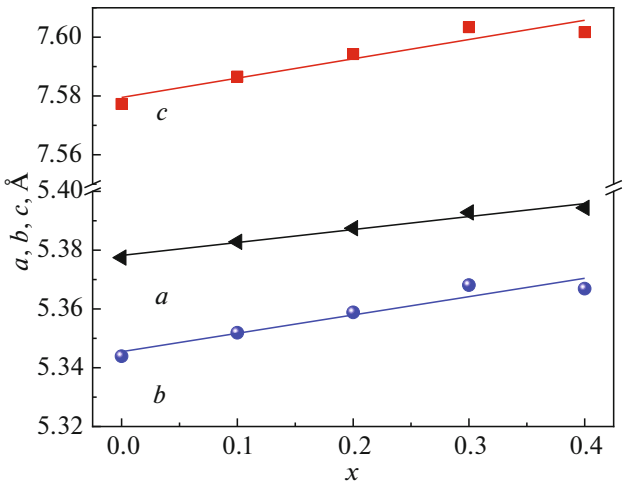


**Fig. 3.** Unit cell parameters of $PrCo_{1-x}Ni_xO_3$ at various nickel content (*x*).

(Fig. 3) suggests that cobalt is in a low-spin state $r(Co^{3+}_{VI}, LS) = 0.545$ Å, $r(Co^{3+}_{VI}, HS) = 0.61$ Å, $r(Ni^{3+}_{VI}, LS) = 0.56$ Å, $r(Ni^{3+}_{VI}, HS) = 0.6$ Å [45].

Examples of XRD patterns for the samples whose composition lies outside the homogeneity range are shown in Fig. 4. It should be noted that at a high nickel content ($x = 0.9$), the perovskite phase is no longer formed, and the coexisting phases are a Ruddlesden–Popper type solid solution with $n = 3$, $Pr_2NiO_4$, and NiO.

### *$Pr_4Ni_{3-y}Co_yO_{10-\delta}$ Solid Solutions*

Although the decomposition temperature of $Pr_4Ni_3O_{10}$ in air is estimated to be approximately 1323 K, partial replacement of nickel by cobalt leads to stabilization of the Ruddlesden–Popper type structure with $n = 3$ at 1373 K. According to the XRD results of quenched samples, single-phase $Pr_4Ni_{3-y}Co_yO_{10-\delta}$ solid solutions were obtained in the composition range $0.7 \le y \le 1.5$. A lower cobalt content in the solid solution ($y = 0.3$) was achieved by the authors of [25, 41] by using lower annealing temperatures ($T = 1223$ K). All obtained solid solutions have a monoclinic structure (sp. gr. $P121/c1$), similar to that reported in the literature for unsubstituted praseodym-

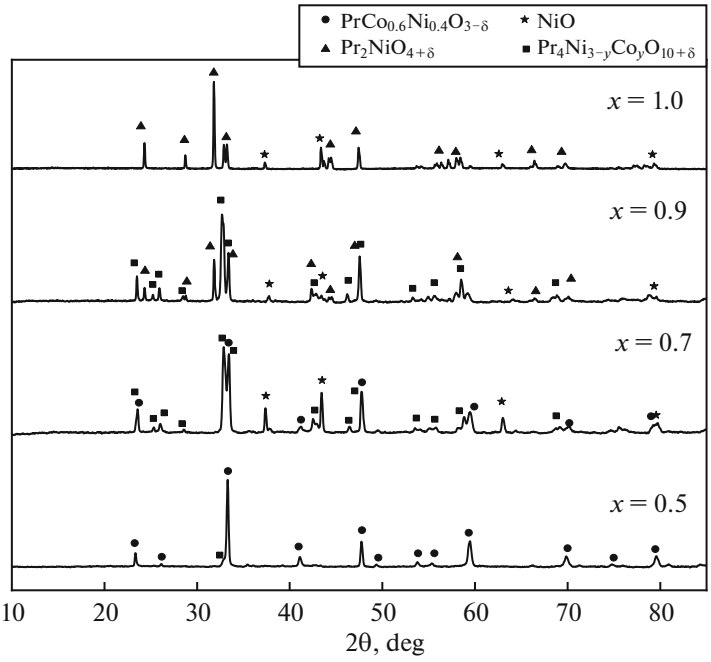


**Fig. 4.** XRD patterns of multi-phase samples with nominal composition $PrCo_{1-x}Ni_xO_3$ at various $x$ values.

ium nickelate $Pr_4Ni_3O_{10}$ [42] and a solid solution with $y = 0.3$ [41]. Studying the effect of temperature on the crystal structure of a solid solution with $y = 0.3$, the authors of [25] found that at $T > 873$ K the monoclinic phase begins to gradually transform into a tetragonal phase (sp. gr. $I4/mmm$), and both phases coexist in a fairly wide temperature range (923–1173 K). Without sufficient grounds to talk about the reasons for this behavior, of which there may be several, Berger et al. [25] chose not to discuss them.

The oxygen content in $Pr_4Ni_{3-y}Co_yO_{10-\delta}$ (Table 2), similar to solid solutions with a perovskite structure, is also not very different from the stoichiometric one, and its change with temperature is also not too large. Table 2 also shows the average oxidation states of 3*d* metals ($z$).

It is obvious that with the simultaneous presence of Co and Ni in the oxide, cobalt ions will predominantly be in the $Co^{3+}$ state, while nickel ions will tend to lower their oxidation state to $Ni^{2+}$. Taking this fact and the oxygen content into account, the formulas of solid solutions were presented as follows:

| 298 K | 1373 K |
|---|---|
| $Pr_4Ni^{2+}_{0.98}Ni^{3+}_{1.32}Co^{3+}_{0.7}O_{10.01}$, | $Pr_4Ni^{2+}_{1.14}Ni^{3+}_{1.16}Co^{3+}_{0.7}O_{9.93}$, |
| $Pr_4Ni^{2+}_{0.94}Ni^{3+}_{1.16}Co^{3+}_{0.9}O_{10.03}$, | $Pr_4Ni^{2+}_{1.04}Ni^{3+}_{1.06}Co^{3+}_{0.9}O_{9.98}$, |
| $Pr_4Ni^{2+}_{0.98}Ni^{3+}_{0.92}Co^{3+}_{1.1}O_{10.01}$, | $Pr_4Ni^{2+}_{1.06}Ni^{3+}_{0.84}Co^{3+}_{1.1}O_{9.97}$, |
| $Pr_4Ni^{2+}_{0.92}Ni^{3+}_{0.88}Co^{3+}_{1.2}O_{10.04}$, | $Pr_4Ni^{2+}_{1.00}Ni^{3+}_{08}Co^{3+}_{1.2}O_{10.00}$, |
| $Pr_4Ni^{2+}_{1.02}Ni^{3+}_{0.58}Co^{3+}_{1.4}O_{9.99}$, | $Pr_4Ni^{2+}_{1.1}Ni^{3+}_{0.5}Co^{3+}_{1.4}O_{9.95}$. |

The crystal structure of oxides of the homologous Ruddlesden–Popper series with $n = 3$ ($A_4B_3O_{10}$) is an alternation of three perovskite blocks ($ABO_3$) and a layer of rock salt (AO) along the $c$ axis. According to the crystallographic approach of the sum of valence

**Table 2.** Oxygen content and average oxidation states of 3*d* metal ions ($z$) in $Pr_4Ni_{3-y}Co_yO_{10-\delta}$ ($y = 0.7$, 0.9, 1.1, 1.2, 1.4) at 298 and 1373 K

| $T$, K | $y$ | 0.7 | 0.9 | 1.1 | 1.2 | 1.4 |
|---|---|---|---|---|---|---|
| 298 | $10 - \delta$ | 10.01(1) | 10.03(1) | 10.01(1) | 10.04(1) | 9.99(1) |
| | $z$ | 2.67(1) | 2.69(1) | 2.67 (1) | 2.69(1) | 2.66(1) |
| 1373 | $10 - \delta$ | 9.93(1) | 9.98(1) | 9.97 (1) | 10.00(1) | 9.95(1) |
| | $z$ | 2.62(1) | 2.65(1) | 2.65(1) | 2.67(1) | 2.63(1) |

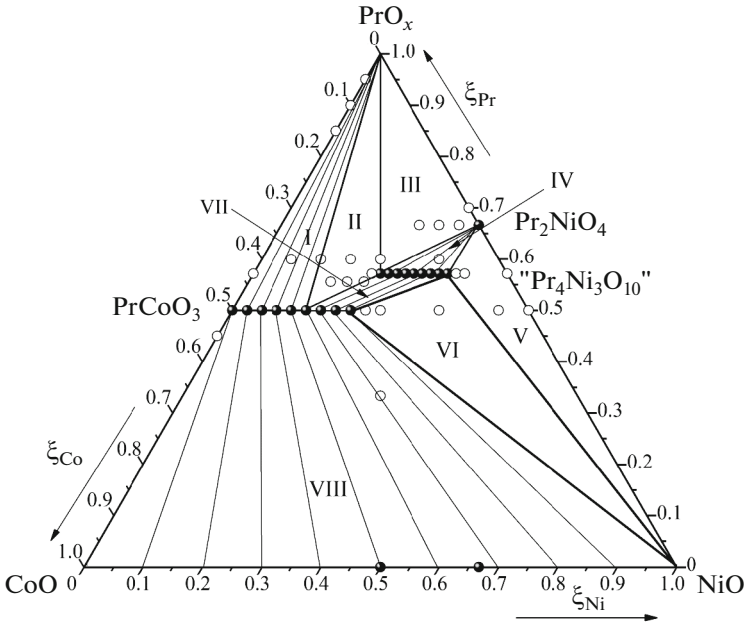


**Fig. 5.** Phase diagram of the $PrO_x$–CoO–NiO system in air at 1373 K and $P_{O_2}$ = 0.21 atm.

bonds method, the distribution of doubly and triply charged cations with simultaneous presence in the oxide is as follows: the former will stay in the center of octahedra located between two layers of perovskite, and the latter—in octahedra located near the rock salt layer. Thus, it should be assumed that $Ni^{2+}$ ions, which content is approximately 1/3 of the total number of cations in B-sites, are located in the "internal" octahedra of the perovskite block. The remaining part of the nickel ions, with a predominant oxidation state of 3+, and $Co^{3+}$ ions are located in the perovskite layers adjacent to the rock salt (AO) layer. The amounts of $Ni^{3+}$ and $Co^{3+}$ ions in these layers are comparable. Since phases with a Ruddlesden–Popper type structure in the $PrO_x$–CoO system are not stable in air (in rare earth and cobalt oxides, the latter, under the studied conditions, tends to take $Co^{3+}$ state and, therefore, form the perovskite structure $LnCo^{3+}O_3$), an increase in the content of ions cobalt in layers near the rock salt layer becomes thermodynamically unfavorable. Further introduction of cobalt into the system leads to separation, and along with the "cobalt-saturated" boundary solution $Pr_4Ni_{1.5}Co_{1.5}O_{10-\delta}$, two more phases are formed: $PrCo_{1-x}Ni_xO_3$ perovskite and $PrO_x$. Thus, the gradual replacement of nickel with cobalt at the first stage stabilizes the $A_4B_3O_{10}$-type structure due to the appearance of triply charged $Co^{3+}$ ions, which, together with nickel ions, fill octahedrons near the rock salt layers. On the other hand, an increase in the proportion of cobalt ions makes it more advantageous to form a perovskite structure, which provides a higher degree of oxidation of 3*d* metals in the B sublattice. Similar observations about the determining role of the nature of 3*d* metals on the stability of certain perovskite-like phases and changes in phase equilibria in systems based on rare earth elements and 3*d* transition metals were reported earlier [46].

**Table 3.** Phase composition of fields in the phase diagram of the $PrO_x$–CoO–NiO system at 1373 K in air

| No. | Composition in the fields of phase diagram |
|---|---|
| I | $PrO_x$, $PrCo_{1-x}Ni_xO_3$ ($0.0 \le x \le 0.25$) |
| II | $PrO_x$, $PrCo_{0.75}Ni_{0.25}O_3$, $Pr_4Ni_{1.5}Co_{1.5}O_{10-\delta}$ |
| III | $PrO_x$, $Pr_2NiO_{4+\delta}$, $Pr_4Ni_{1.5}Co_{1.5}O_{10-\delta}$ |
| IV | $Pr_2NiO_{4+\delta}$, $Pr_4Ni_{3-y}Co_yO_{10-\delta}$ ($0.7 \le y \le 1.5$) |
| V | $Pr_2NiO_{4+\delta}$, NiO, $Pr_4Ni_{2.3}Co_{0.7}O_{10-\delta}$ |
| VI | $Pr_4Ni_{2.3}Co_{0.7}O_{10-\delta}$, NiO, $PrCo_{0.6}Ni_{0.4}O_3$ |
| VII | $Pr_4Ni_{3-y}Co_yO_{10-\delta}$ ($0.7 \le y \le 1.5$), $PrCo_{1-x}Ni_xO_3$ ($0.25 \le x \le 0.4$) |
| VIII | $PrCo_{1-x}Ni_xO_3$ ($0.0 \le x \le 0.4$), $Co_{1-z}Ni_zO$ ($0.0 \le z \le 1.0$) |

### *Phase Diagram of the $PrO_x$–CoO–NiO System at 1373 K in Air*

An analysis of phase equilibria in the $PrO_x$–CoO–NiO system at 1373 K in air was carried out based on the XRD results of 47 quenched samples. The phase

diagram in the form of a Gibbs triangle is shown in Fig. 5. Here, as in quasi-binary systems, the composition is presented in terms of the relative mole fraction of metal components. The phase composition in the fields of phase diagram is presented in Table 3.

The composition of the $PrCo_{1-x}Ni_xO_3$ solid solution, dividing it into a part coexisting with $PrO_x$ and a part coexisting with $Pr_4Ni_{3-y}Co_yO_{10-\delta}$, was determined from the unit cell parameters of the perovskite phase in samples from field II and the concentration dependence of the solid solution unit cell parameters (Fig. 3).

Attempts to partially replace nickel with cobalt in $Pr_2NiO_{4+\delta}$ at 1373 K in air were unsuccessful. The phase composition of all studied samples corresponded to field III of the phase diagram (Fig. 5). It is likely that the preparation of such solutions with a noticeable content of cobalt $Pr_2Ni_{1-y}Co_yO_{4+\delta}$ will be possible under more reducing conditions (high temperatures and/or lower $P_{O_2}$ values relative to air).

A comparison of the phase equilibria in the studied system and a similar one based on lanthanum $1/2La_2O_3$–CoO–NiO [47] reveals a number of analogies, although there are some differences. The differences are associated with the stability of the Ruddlesden–Popper homologous series phases for different REEs. Three homologues are stable in the lanthanum-containing system at 1373 K in air: $La_2NiO_4$, $La_3Ni_2O_7$, and $La_4Ni_3O_{10}$ [48–50], therefore, solid solutions with partial replacement of nickel by cobalt start from the $1/2La_2O_3$–NiO side. As a result, the homogeneity ranges of such solid solutions are somewhat wider compared to the Pr-containing system: for $La_2Ni_{1-y}Co_yO_{4+\delta}$ $y_{max} = 0.1$, for $La_4Ni_{3-y}Co_yO_{10}$ $y_{max} = 1.8$. Phase equilibria in the $1/2Sm_2O_3$–CoO–NiO system [51] with smaller REE confirms the observed trend. The only stable intermediate phase in it is $SmCo_{1-x}Ni_xO_3$ with a homogeneity range of $0 \le x \le 0.15$ [51], while for $LaCo_{1-x}Ni_xO_3$ it is $0 \le x \le 0.6$ [47], and for $PrCo_{1-x}Ni_xO_3$ it has an intermediate value ($0.0 \le x \le 0.4$).

## CONCLUSIONS

Analysis of phase equilibria in the $PrO_x$–CoO–NiO system at 1373 K in air showed the presence of two series of solid solutions: $PrCo_{1-x}Ni_xO_3$ ($0.0 \le x \le 0.4$) with the structure of an orthorhombically distorted perovskite and $Pr_4Ni_{3-y}Co_yO_{10-\delta}$ ($0.7 \le y \le 1.5$) with the Ruddlesden–Popper ($n = 3$) structure. There is no noticeable substitution of nickel for cobalt in praseodymium nickelate $Pr_2NiO_{4+\delta}$ under these conditions. The obtained solid solutions are practically stoichiometric in oxygen. An increase in the unit cell parameters of $PrCo_{1-x}Ni_xO_3$ with increasing nickel content may indirectly indicate that cobalt ions are in a low-spin state. In the $Pr_4Ni_{3-y}Co_yO_{10-\delta}$ structure, $Ni^{2+}$ ions are settled in octahedra located in the middle of the perovskite block, while $Ni^{3+}$ and $Co^{3+}$ are placed in octahedra adjacent to the rock salt layer.

## FUNDING

The work was supported by the Ministry of Science and Higher Education of the Russian Federation (project no. 123031300049-8).

## CONFLICT OF INTEREST

The authors of this work declare that they have no conflicts of interest.

## REFERENCES

1. M. A. Morales-Zapata, A. Larrea, and M. A. Laguna-Bercero, Electrochim. Acta **444**, 141970 (2023).
2. V. Vibhu, A. Flura, C. Nicollet, et al., Solid State Sci. **81**, 26 (2018). https://doi.org/10.1016/j.solidstatesciences.2018.04.016
3. V. Vibhu, A. Rougier, C. Nicollet, et al., J. Power Sources **317**, 184 (2016). https://doi.org/10.1016/j.jpowsour.2016.03.012
4. Y. Miyamoto, A. Nagai, S. Nishimoto, et al., Mater. Lett. **349**, 134731 (2023). https://doi.org/10.1016/j.matlet.2023.134731
5. D. D. Mishchenko, M. V. Arapova, Y. N. Bespalko, et al., J. Alloys Compd. **967**, 171693 (2023). https://doi.org/10.1016/j.jallcom.2023.171693
6. A. Egger, S. Eisbacher-Lubensky, K. Sampl, et al., Fuel Cells, 1 (2023). https://doi.org/10.1002/fuce.202300037
7. S. Vafaeenezhad, M. A. Morales-Zapata, A. R. Hanifi, et al., Int. J. Hydrogen Energy **47**, 35081 (2022). https://doi.org/10.1016/j.ijhydene.2022.08.108
8. E. P. Antonova, A. V. Khodimchuk, E. S. Tropin, et al., Solid State Ionics **346**, 115215 (2020). https://doi.org/10.1016/j.ssi.2019.115215
9. C.-Y. Tsai, A. Aguadero, and S. J. Skinner, J. Solid State Chem. **289**, 121533 (2020). https://doi.org/10.1016/j.jssc.2020.121533
10. J.-M. Bassat, V. Vibhu, C. Nicollet, et al., ECS Trans. **78**, 655 (2017). https://doi.org/10.1149/07801.0655ecst
11. X.-D. Zhou, J. W. Templeton, Z. Nie, et al., Electrochim. Acta **71**, 44 (2012). https://doi.org/10.1016/j.electacta.2012.03.067
12. Z. Xie, I. Jang, M. Ouyang, et al., J. Phys. Energy **5**, 045005 (2023). https://doi.org/10.1088/2515-7655/aceeb5
13. A. V. Kovalevsky, V. V. Kharton, A. A. Yaremchenko, et al., J. Electroceram. **18**, 205 (2007). https://doi.org/10.1007/s10832-007-9024-7

14. V. Vibhu, I. C. Vinke, R.-A. Eichel, and L. G. J. de Haart, J. Power Sources **482**, 228909 (2021). https://doi.org/10.1016/j.jpowsour.2020.228909
15. V. Vibhu, I. C. Vinke, R.-A. Eichel, et al., J. Power Sources **444**, 227292 (2019). https://doi.org/10.1016/j.jpowsour.2019.227292
16. S. I. Sozal Md, W. Tang, S. Das, et al., Int. J. Hydrogen Energy **47**, 21817 (2022). https://doi.org/10.1016/j.ijhydene.2022.05.011
17. T. V. Aksenova, L. Ya. Gavrilova, and V. A. Cherepanov, Inorg. Mater. **40**, 1336 (2004).
18. S. Huang, Q. Lu, S. Feng, et al., J. Power Sources **199**, 150 (2012). https://doi.org/10.1016/j.jpowsour.2011.10.025
19. V. A. Sadykov, N. F. Eremeev, E. M. Sadovskaya, A. S. Bobin, Yu. E. Fedorova, V. S. Muzykantov, N. V. Mezentseva, G. M. Alikina, T. A. Kriger, V. D. Belyaev, V. A. Rogov, A. S. Ulikhin, Yu. S. Okhlupin, N. F. Uvarov, O. F. Bobrenok, et al., Russ. J. Electrochem. **50**, 669 (2014). https://doi.org/10.1134/S1023193514070131
20. V. Sadykov, N. Eremeev, E. Sadovskaya, et al., Catal. Today **423**, 113936 (2023). https://doi.org/10.1016/j.cattod.2022.10.018
21. C. Berger, E. Bucher, A. Egger, et al., Solid State Ionics **316**, 93 (2018). https://doi.org/10.1016/j.ssi.2017.12.024
22. A. A. Yaremchenko, V. V. Kharton, M. V. Patrakeev, and J. R. Frade, J. Mater. Chem. **13**, 1136 (2003). https://doi.org/10.1039/b300357d
23. S. Li, H. Tu, F. Li, et al., J. Alloys Compd. **694**, 17 (2017). https://doi.org/10.1016/j.jallcom.2016.09.250
24. A. P. Tarutin, A. V. Kasyanova, G. K. Vdovin, et al., Materials **15**, 2166 (2022). https://doi.org/10.3390/ma15062166
25. C. Berger, E. Bucher, R. Merkle, et al., Open Ceram. **6**, 100094 (2021). https://doi.org/10.1016/j.oceram.2021.100094
26. V. A. Cherepanov, A. N. Petrov, and L. Yu. Grimova, Zh. Fiz. Khim. **59**, 2131 (1985).
27. A. N. Petrov, V. A. Cherepanov, A. Yu. Zuyev, and V. M. Zhukovsky, J. Solid State Chem. **77**, 1 (1988). https://doi.org/10.1016/0022-4596(88)90083-7
28. K. Kitayama, J. Solid State Chem. **77**, 366 (1988). https://doi.org/10.1016/0022-4596(88)90260-5
29. K. Kitayama, J. Solid State Chem. **151**, 12 (2000). https://doi.org/10.1006/jssc.1999.8602
30. G. Ch. Kostogloudis, N. Vasilakos, and Ch. Ftikos, Solid State Ionics **106**, 207 (1998). https://doi.org/10.1016/S0167-2738(97)00506-7
31. P. Lacorre, J. B. Torrance, J. Pannetier, et al., J. Solid State Chem. **91**, 225 (1991). https://doi.org/10.1016/0022-4596(91)90077-U
32. T. C. Huang, W. Parrish, H. Toraya, et al., Mater. Res. Bull. **25**, 1091 (1990). https://doi.org/10.1016/0025-5408(90)90138-R
33. X. Q. Xu, J. L. Peng, Z. Y. Li, et al., Phys. Rev. B **48**, 1112 (1993). https://doi.org/10.1103/PhysRevB.48.1112
34. J. E. Rodrigues, A. D. Rosa, J. López-Sánchez, et al., J. Mater. Chem. C **11**, 462 (2023). https://doi.org/10.1039/d2tc03063b
35. J. M. Bassat, C. Allançon, P. Odier, et al., Eur. J. Solid State Inorg. Chem. **35**, 173 (1998). https://doi.org/10.1016/S0992-4361(98)80195-1
36. F. M. Aquino, D. M. A. Melo, P. M. Pimentel, et al., Mater. Res. Bull. **47**, 2605 (2012). https://doi.org/10.1016/j.materresbull.2012.04.078
37. P. Odier, Ch. Allançon, and J. M. Bassat, J. Solid State Chem. **153**, 381 (2000). https://doi.org/10.1006/jssc.2000.8786
38. A. V. Kovalevsky, V. V. Kharton, A. A. Yaremchenko, et al., J. Eur. Ceram. Soc. **27**, 4269 (2007). https://doi.org/10.1016/j.jeurceramsoc.2007.02.136
39. E. Takayama, J. Solid State Chem. **50**, 70 (1983). https://doi.org/10.1016/0022-4596(83)90233-5
40. P. Tomeš, M. H. Aguirre, R. Robert, et al., J. Phys. D: Appl. Phys. **44**, 305402 (2011). https://doi.org/10.1088/0022-3727/44/30/305402
41. C. Berger, E. Bucher, A. Egger, et al., Solid State Ionics **348**, 115282 (2020). https://doi.org/10.1016/j.ssi.2020.115282
42. J. Song, D. Ning, B. Boukamp, et al., J. Mater. Chem. A **8**, 22206 (2020). https://doi.org/10.1039/d0ta06731h
43. E. Dogdibegovic, C. J. Wright, and X.-D. Zhou, J. Am. Ceram. Soc. **99**, 2737 (2016). https://doi.org/10.1111/jace.14291
44. A. N. Petrov, V. A. Cherepanov, and A. Yu. Zuev, Zh. Fiz. Khim. **61**, 630 (1987).
45. R. D. Shannon, Acta Crystallogr., A **32**, 751 (1976). https://doi.org/10.1107/S0567739476001551
46. V. A. Cherepanov, L. Yu. Barkhatova, and A. N. Petrov, J. Phys. Chem. Solids **55**, 229 (1994). https://doi.org/10.1016/0022-3697(94)90137-6
47. L. Ya. Gavrilova, N. V. Proskurnina, V. A. Cherepanov, and V. I. Voronin, in *Solid Oxide Fuel Cells VII, PV 2001-16,* Ed. by H. Yokokawa and S. C. Singhal, *Electrochemical Society Proceedings Series* (Electrochem. Soc., Pennington, NJ, 2001), p. 458.
48. D. O. Bannikov and V. A. Cherepanov, J. Solid State Chem. **179**, 2721 (2006). https://doi.org/10.1016/j.jssc.2006.05.026
49. M. Zinkevich, N. Solak, H. Nitsche, et al., J. Alloys Compd. **438**, 92 (2007). https://doi.org/10.1016/j.jallcom.2006.08.047
50. M. Zinkevich and F. Aldinger, J. Alloys Compd. **375**, 147 (2004). https://doi.org/10.1016/j.jallcom.2003.11.138
51. A. P. Galayda, N. E. Volkova, L. Ya. Gavrilova, and V. A. Cherepanov, Inorg. Mater. **55**, 593 (2019). https://doi.org/10.1134/S0020168519060049